Wireless Reading of Additively Manufactured Galinstan-based Sensor using a Polarimetric Millimeter-wave Radar Imaging Technique

Dominique Henry, Ahmad El Sayed Ahmad, Ali Hadj Djilani, Patrick Pons, Hervé Aubert

Wireless Reading of Additively Manufactured Galinstan-based Sensor using a Polarimetric Millimeter-wave Radar Imaging Technique

Dominique Henry[#1], Ahmad El Sayed Ahmad[#], Ali Hadj Djilani[#], Patrick Pons[#], Hervé Aubert[#]
[#]LAAS-CNRS, Toulouse University, France
[1]dhenry@laas.fr

***Abstract* — A polarimetric millimeter-wave radar imaging technique is proposed to wirelessly read a novel additively manufactured passive sensor composed of a microfluidic channel filled with liquid metal Galinstan. Very high variation of the radar-cross section of the sensor to small variations of the level of Galinstan in the channel is obtained. Indeed, at the radar-to-sensor distance of 2.4m, the measured radar echo level of the sensor varies by 4.5dB when the level of Galinstan changes by 1mm. This sensitivity is higher than previously reported in the Literature for wireless and passive sensors of the same class.**

***Keywords* — additive manufacturing, Galinstan, liquid metal, polarimetry, radar imagery, remote monitoring, sintering laser melting.**

I. Introduction

Remote interrogation of wireless sensors is sometimes challenging, especially in industrial applications or harsh environments where human intervention, wiring and/or battery replacement are not possible. In such environments, the use of passive and chipless sensors (i.e. sensors without battery and integrated circuits) may be a suitable solution. Such devices, designated as chipless radio-frequency identification (RFID) sensors, are still today a research topic of great interest with issues related to multi-sensing [1], bio-compatibility [2], data density [3] or field polarization [4]. The counterpart is that the range of the wireless interrogation may be too short for many applications: the maximal reader-to-sensor distance of interrogation is typically 1 meter for chipless RFID sensors to comply with effective isotropic radiated power (EIRP) standards [5]. Moreover, the sensors often present both minimal measurement sensitivity and minimal full-scale (or dynamic) range, depending on the targeted application. A solution to increase both the dynamic range and the reader-to-sensor distance is to use a FM-CW (Frequency-Modulated Continuous-Wave) radar with directive receiving and transmitting antennas in order to perform longer reader-to-sensor separation distances [6]. A 3D beamscanning method combined with a dedicated radar image processing was also recently proposed [7]. Because industrial and harsh environments are often very reflective for RF waves, the remote reading of wireless sensors may be altered by the electromagnetic clutter. For this reason, efforts have been recently undertaken to increase the signal-to-noise ratio (SNR) by designing depolarizing chipless sensors [8] and to reach reader-to-sensor separation distance of five decades of meters [9]. A multi-sensor remote-reading approach in industrial environment was also proposed in [10] using chipless pressure sensors manufactured from clean room technological facilities. The main issue of such sensors was their low measurement dynamic range, as their operating frequency was found to be slightly outside the radar modulation bandwidth. Moreover, these sensors required the use of delay lines (coaxial cables) that may be not suitable for cost-effective and flexible multi-sensing approach in many practical applications. In this context, a cost-effective pressure chipless sensor was fabricated from additive manufacturing technology and microfluidic technology [11]. However, as the liquid was water in the first reported prototype, the proposed technological solution is not suitable for wide-range temperature measurement, especially below 0°C at atmospheric pressure. Moreover, the metallic hollow waveguide technology printed from Sintering Laser Melting (SLM) technique was applied in [11] for 3D printing of only part of the wireless sensor and not the entire structure (the two cross-polarized sensor antennas and delay lines were actually not 3D printed).

In this paper the SLM technique is applied in Section II to entirely fabricate the passive sensor composed of a microfluidic channel filled with liquid metal Galinstan. It has a thermal expansion coefficient of $11.5\times10^{-5}\mathrm{K}^{-1}$ [12] at room temperature and can be used for the remote sensing of temperature variation [13]. In Section III, we investigate the wireless interrogation of the proposed additively manufactured Galinstan-based sensor. It is shown that the level of Galinstan in the sensor's channel can be accureatly estimated from the processing of isolines in polarimetric millimeter-wave radar images.

II. Passive and Wireless Microfluidic Sensor

A. Design and Simulation

The proposed wireless and passive microfluidic sensor is a metallic waveguide structure composed of an electromagnetic transducer connected to two cross-polarized antennas. The schematic of the structure is displayed in Fig 1a. Dimensions of the cavity cross-section are those of a standard *WR28* rectangular waveguide (3.556mm×7.112mm). A detailed view of the electromagnetic transducer is displayed in Fig 1b. One port of the cavity is connected to a vertically (V) polarized horn antenna. The second port of the cavity is connected to a (H) horizontally polarized horn antenna by using a bend (H-plane) rectangular waveguide followed by a 90° twisted rectangular waveguide. Such structure is designed to operate in the frequency bandwidth ranging from 22.8GHz to 24.8GHz and its dimensions are of 74.9mm×69.8mm×31.8mm. Simulated gain of the two horn

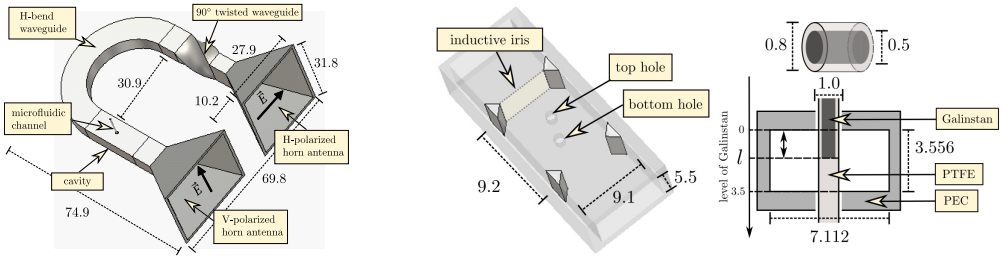

(a) (b) (c)

Fig. 1. (a) 3D schematic of the passive microfluidic sensor metallic structure. (b) Detailed view of the cavity. (c) Cross-sectional view of the microfluidic channel in the rectangular waveguide. Units are in mm.

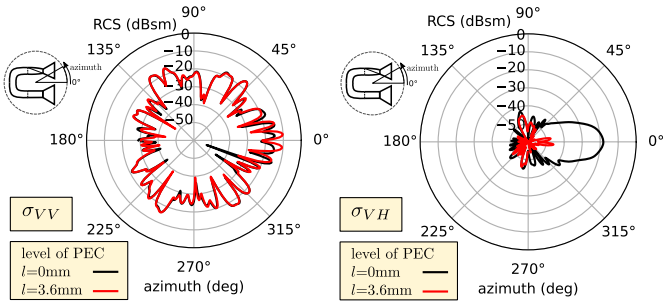

(a) (b)

Fig. 2. Simulated monostatic RCSs of the structure vs azimuth angle: (a) co- and (b) cross-polarized RCSs σ_{VV} and σ_{VH}. Black and red diagrams refer respectively to l=0mm (fluidic channel is empty) and l=3.6mm (channel is completely filled with metal liquid).

antennas at 23.8GHz is 15.5dBi and the half-power beamwidth is 25° in the E-plane and 31° in the H-plane. To be compliant with additive manufacturing technology, the two irises placed at the input and output of the cavity are triangular in shape. The cavity is crossed by a polytetrafluoroethylene (PTFE, relative permittivity of 2.1) microfluidic channel (internal diameter of 500μm and external diameter of 800μm) from two holes at top and bottom of the metallic structure. Inside the channel flows the liquid metal Galinstan. The microfluidic channel crosses the cavity at its center, where the electric field of the fundamental resonant mode reaches its highest magnitude. A detailed view of the microfluidic channel with Galinstan through the waveguide is displayed in Fig 1c. The meniscus position l of Galinstan in the channel is called here "*the level of Galinstan*". When this level is of 0mm, it means that the microchannel placed inside the cavity is empty; when the level equals to the height of the waveguide (i.e. when l=3.556mm), the channel inside the waveguide structure is completely filled with Galinstan.

Port 1 of the cavity is connected to the V-polarized horn antenna while port 2 is connected to the H-polarized horn antenna by using the H-bend rectangular waveguide followed by the 90° twisted rectangular waveguide. The simulated monostatic Radar Cross Sections (RCSs) σ_{VV} and σ_{VH} of the structure are displayed in Fig 2 as a function of the azimuth angle and for two levels of Galinstan : l=0mm and l=3.6mm. As the structure converts (thanks to its 90° twisted waveguide) the incident V-polarized field into a reradiated H-polarized field, the (simulated) dynamic range offered by σ_{VH} (32dB) is much higher that one achieved by σ_{VV} (5dB).

B. Fabrication and Measurement

The prototype of the microfluidic passive sensor is entirely fabricated from the SLM technique. The metal powder is stainless steel (316L with an electrical conductivity of 3.10^6 S/m and an average roughness of 7μm). For practical reasons, the metallic structure is manufactured in five parts: the cavity, one single horn antenna, one horn antenna with the 90° twisted waveguide and two sections of H-bend antenna. Flanges are added at waveguide terminations to assemble the different parts of the structure. The photograph of the resulting 3D printed sensor is shown in Fig 3a.

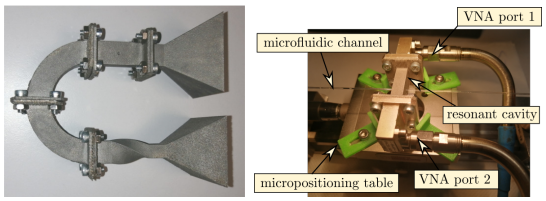

(a) (b)

Fig. 3. (a) Micro-positioning table for the S-parameters measurement of the two-port cavity. (b) Photograph of additively manufactured 3D structure (without the microfluidic part).

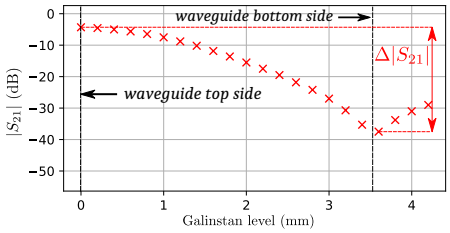

Fig. 4. Measured transmission coefficient at 23.8GHz as a function of the level of metal liquid.

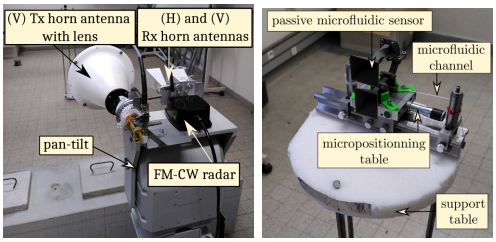

(a) (b)

Fig. 5. (a) Photograph of the 3D beamscanning. (b) Photograph of the passive microfluidic sensor set on the micro-positioning table.

Magnitude of the transmission coefficient S_{21} is measured by using a Vector Network Analyzer for various levels of Galinstan. To control the level of Galinstan, the experimental setup shown in Fig 3b is used: the cavity, crossed by the PTFE channel filled with Galinstan, is set on a micro-positioning table that performs translations with a displacement precision of few μm. The channel is static and both ends are sealed. The initial level of Galinstan is set with a microscope at the top edge of the metallic structure. Therefore, the level of Galinstan is 0mm when the cavity is translated over the waveguide thickness (1.0mm). When the micro-positioning table displaces the cavity along the channel, the level of Galinstan increases. We note that the uncertainty of the waveguide thickness is of $\pm 20\mu m$, and the curvature in the meniscus of the liquid metal induced an uncertainty of $10\mu m$ on the level l of the Galinstan. Therefore, the level of Galinstan is estimated with a precision of $\pm 30\mu m$ during the displacement of the cavity along the (static) channel. The measured magnitude of the transmission coefficient as a function of the level of Galinstan is displayed in Fig 4 (red color). Difference between the (lossless) simulation results and experimental data does not exceed 5dB. We obtain a measured full dynamic range $\Delta|S_{21}|$=33dB, and consequently, a measured sensitivity $\Delta|S_{21}|/\Delta_l$ of 9.1dB/mm. Between 0.8mm to 3.0mm, the sensitivity is slightly higher (9.3dB/mm).

III. Polarimetric Radar Imaging of Passive and Wireless Microfluidic Sensor

A. Experimental Setup

A 3D beamscanning is performed using a FM-CW radar with carrier frequency f_c of 24.3GHz and modulation bandwidth B of 2GHz. As a result, the so-called theoretical depth resolution d=$\frac{c}{2B}$ (where c is the speed of light in vacuum) is found to be of 7.5cm. The radar front-end is composed of one transmitting channel (T_x) and two receiving (R_x) channels (model DK-sR-1030e from IMST GmbH [14]). The microwave power (20dBm) transmitted by the radar through a lens-loaded vertically polarized (V-polarized) circular horn antenna (gain of 28dBi and half-beamwidth of 6°). The receiving antennas are respectively V- and H-polarized rectangular horn antennas (gain of 20dBi). At a distance of 2.4m from the radar is located the depolarizing passive microfluidic sensor. The sensor operates in the frequency bandwidth of the radar, and its radar echo depends on the level l of Galinstan. The 3D beamscanning is performed mechanically by using a pan-tilt that allows steering the main beam of the radar T_x-antenna with the azimuth (φ) sweep of $\pm 10°$ and angular speed v_φ=4° per second. Since the chirps are transmitted with the repetition time t_{rep}=53ms, the azimuth angular step is d_φ=$v_\varphi \times t_{rep}$=0.2°. The main beam sweep in elevation is of $\pm 10°$ with the angular step of 1°. A photograph of the radar mounted on the mechanical platform is shown in Fig 5a.

The microfluidic passive sensor is located in a room of our Laboratory and placed at the distance of 2.4m from the radar and the sensor is set on a micro-positioning table in which the microfluidic channel filled with Galinstan is integrated. As previously indicated, the microfluidic channel crosses the metallic structure through the rectangular waveguide cavity (see Fig 5b). Beamscannings are performed for level l of Galinstan ranging from 0mm to 4.6mm through the channel with a step of 0.2mm. In each direction (θ, φ) in space, the chirp is transmitted by the radar and the beat frequency spectrum is obtained in this direction. Each spectrum is composed of N_R=256 samples and the maximal radar interrogation distance d_{max} is then given by $d \times N_R$. The resulting 3D image after a beamscanning is a matrix of size $N_\theta \times N_\varphi \times N_s$, where N_θ=21 and N_φ=105 are respectively the number of samples in elevation and azimuth angles. Moreover, the radar images are obtained from four configurations of polarizations p that are defined by the polarizations of the transmitting and receiving antennas. Indeed p=VV (or VH) if the measurement is performed by using a V-polarized transmitting antenna and a V- (or H-) polarized receiving

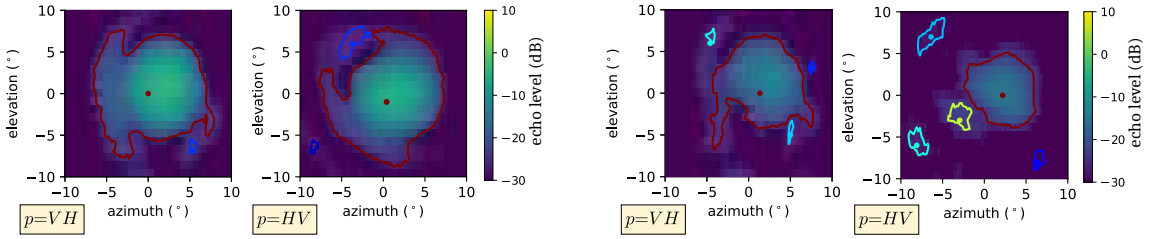

Fig. 6. Radar images in the (θ, φ) at the reader-to-sensor position R=2.4m for cross-polarization configurations and for a level of Galinstan of (a) 0mm and (b) 3.0mm inside the channel.

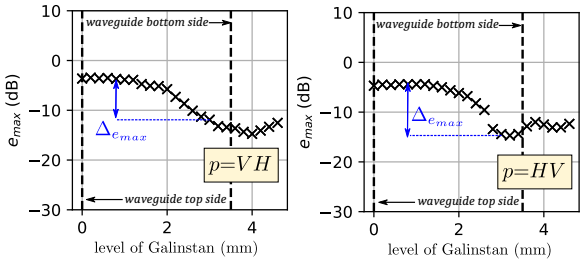

Fig. 7. Statistical estimator e_{max} as a function of the level of Galinstan inside the microfluidic channel with polarization configurations (a) VH, and (b) HV for a microfluidic passive sensor located at 2.4m in front of the radar. The dynamic range $\Delta_{e_{max}}$ is plotted from l=0.8mm to l=3.0mm.

antenna; equivalently, if the experiment is performed by using H-polarized transmitting antenna and V- (or H-) polarized receiving antenna, then p=HV (or p=HH).

B. Wireless Reading from Polarimetric Radar Imaging Technique

The polarimetric radar images provided by the two cross-polarization configurations p=VH and HV at the radar-to-sensor distance of 2.4m are displayed in Fig 6 for levels of Galinstan inside the channel of (a) 0.0mm and (b) 3.0mm. Blue to yellow colors represent low (-30dB) to high echo levels (10dB). As expected from the design of the passive sensor, the radar echo level depends on the level of Galinstan in the channel and high echo variation is obtained from the cross-polarized configurations VH and HV. To characterize the variation of echo level when the level of Galinstan changes, we segment radar images with *isolines*. An isoline refers to a line along which the radar echo magnitude is unchanged. The threshold of echo level is adaptive, such as radar echoes from low to high echo levels can be segmented. Features, such as the maximum of echo level e_{max}, are then extracted from isolines and are used to define a statistical estimator for Galinstan level inside the microfluidic channel (see Fig 7). The dynamic range $\Delta_{e_{max}}$ associated to the estimator e_{max} is defined as follows:

$$\begin{aligned}\Delta_{e_{max}} &= |e_{max}(l_{max}) - e_{max}(l_{min})| \\ &= \alpha_{e_{max}}|l_{max} - l_{min}|\end{aligned} \tag{1}$$

where l denotes the level of Galinstan to be estimated, $e_{max}(l_{min})$ and $e_{max}(l_{max})$ denote respectively the measured minimum and maximum of (co- or cross-polarized) echo level at the sensor location for the lowest (l_{min}) and highest (l_{max}) levels of Galinstan and, $\alpha_{e_{max}}$ designates the mean sensitivity of the sensor derived from the statistical estimator e_{max}. The sensitivities are high for cross-polarized configurations (3.7dB/mm for p=VH and 4.5dB/mm for p=HV), and as expected, they are much lower in the co-polarized configurations (0.8dB/mm for p=VV and 2.4dB/mm for p=HH). However, the measured dynamic range is lower than the simulated RCS dynamic range. This difference can be explained by impedance mismatch between the different parts of the printed structure due to misalignments of flanges. Such mismatch can be suppressed by the one-piece manufacturing of the entire sensor. Nevertheless, this sensor offers higher measurement dynamic and sensitivity than those reported in Table 1. Moreover, the minimal detectable variation of the level of Galinstan δ_{min} can also be derived from the standard deviation of the estimator e_{max}. Values of δ_{min} ranging from 3μm to 84μm depending on the sensitivity $\alpha_{e_{max}}$ and the configuration p.

IV. Conclusion

The proposed wireless and passive sensor shows very encouraging results for a first prototype because of its large measurement dynamic range. Based on these results, works are now focused on the additive fabrication of the sensor with Sintering Laser Melting in one single piece in order to remove the flanges and consequently, to suppress impedance mismatch between the different parts of the printed structure due to misalignments. Moreover, investigations are ongoing to extend the proposed polarimetric radar imaging technique to locate the sensor in cluttered environments for reading distances up to few tens of meters.

ref	sensitivity	dynamic range	parameters [a]
[6]	0.4dBm/°C	4dBm	copol; 2m ; 30GHz ; 23dBm
[7]	0.16dB/°C	4.4dB	copol; 2.4m ; 24GHz ; 53.5dBm
[9]	-0.2dB/%RH	9.5dB	xpol; 2.1m ; 24GHz ; 53.5dBm
[10]	3.8dB/bar	3.4dB	xpol; 4.8m ; 24GHz ; 38dBm
[11]	0.03dB/mbar	8.0dB	xpol; 3.0m ; 24GHz ; 48dBm
[13]	0.45dBsm/K	9dBsm	copol; 1.6m ; 30GHz ; 23dBm
this work	4.5dB/mm	9.9dB	xpol; 2.4m ; 24GHz ; 48dBm

a : polarization configuration; reading range; operating frequency; reader EIRP

Table 1. Performances comparison between chipless sensors interrogated by FM-CW radars.

REFERENCES

[1] F. Requena, N. Barbot, D. Kaddour, and E. Perret, "Combined Temperature and Humidity Chipless RFID Sensor," *IEEE Sensors Journal*, vol. 22, no. 16, pp. 16 098–16 110, 2022.

[2] P. Fathi, S. Bhattacharya, and N. C. Karmakar, "Dual-Polarized Keratin-Based UWB Chipless RFID Relative Humidity Sensor," *IEEE Sensors Journal*, vol. 22, no. 3, pp. 1924–1932, 2022.

[3] F. Paredes, C. Herrojo, R. Escudé, E. Ramon, and F. Martín, "High Data Density Near-Field Chipless-RFID Tags With Synchronous Reading," *IEEE Journal of Radio Frequency Identification*, vol. 4, no. 4, pp. 517–524, 2020.

[4] N. Barbot and E. Perret, "Impact of the Polarization over the Read Range in Chipless RFID," in *2021 IEEE International Conference on RFID Technology and Applications (RFID-TA)*, 2021, pp. 139–141.

[5] N. Barbot, O. Rance, and E. Perret, "Classical RFID Versus Chipless RFID Read Range: Is Linearity a Friend or a Foe?" *IEEE Transactions on Microwave Theory and Techniques*, vol. 69, no. 9, pp. 4199–4208, 2021.

[6] S. Bouaziz, F. Chebila, A. Traille, P. Pons, H. Aubert, and M. M. Tentzeris, "Novel microfluidic structures for wireless passive temperature telemetry medical systems using radar interrogation techniques in ka-band," *IEEE Antennas and Wireless Propagation Letters*, vol. 11, pp. 1706–1709, 2012.

[7] D. Henry, H. Aubert, and P. Pons, "3D Scanning and Sensing Technique for the Detection and Remote Reading of a Passive Temperature Sensor," in *2016 IEEE MTT-S International Microwave Symposium (IMS)*, 2016, pp. 1–4.

[8] J. G. Hester and M. M. Tentzeris, "Inkjet-printed Van-Atta reflectarray sensors: A new paradigm for long-range chipless low cost ubiquitous Smart Skin sensors of the Internet of Things," in *2016 IEEE MTT-S International Microwave Symposium (IMS)*, 2016, pp. 1–4.

[9] D. Henry, J. G. D. Hester, H. Aubert, P. Pons, and M. M. Tentzeris, "Long-Range Wireless Interrogation of Passive Humidity Sensors Using Van-Atta Cross-Polarization Effect and Different Beam Scanning Techniques," *IEEE Transactions on Microwave Theory and Techniques*, vol. 65, no. 12, pp. 5345–5354, 2017.

[10] D. Henry, T. Marchal, J. Philippe, P. Pons, and H. Aubert, "Classification of Radar Echoes for Identification and Remote Reading of Chipless Millimeter-Wave Sensors," *IEEE Transactions on Microwave Theory and Techniques*, vol. 69, no. 1, pp. 926–937, 2021.

[11] T. Marchal, D. Henry, P. Pons, and H. Aubert, "Wireless Measurement of the Pressure from the Ka-Band Radar Echo of a 3D-Printed Microfluidic Depolarizing Sensor," in *2021 IEEE MTT-S International Microwave Symposium (IMS)*, 2021, pp. 173–175.

[12] M. Knoblauch, J. M. Hibberd, J. C. Gray, and A. J. van Bel, "A Galinstan Expansion Femtosyringe for Microinjection of Eukaryotic Organelles and Prokaryotes," *Nature Biotechnology*, vol. 17, pp. 906–909, 1999.

[13] A. Traille, S. Bouaziz, S. Pinon, P. Pons, H. Aubert, A. Boukabache, and M. Tentzeris, "A wireless passive RCS-based temperature sensor using liquid metal and microfluidics technologies," in *2011 41st European Microwave Conference*, 2011, pp. 45–48.

[14] "IMST Radar small and flexible radar modules by IMST," http://www.radar-sensor.com/, accessed: 2022-09-26.